Indolent Enhancing Spinal Lesions Mimicking Spinal Metastasis in Pediatric Patients With Malignant Primary Brain Tumors

Hsin-Wei Wu
Department of Radiology, Taipei Veterans General Hospital, Taipei, Taiwan
Shih-Chieh Lin
Department of Pathology and Laboratory Medicine, Taipei Veterans General Hospital, Taipei, Taiwan
Ching-Lan Wu
Department of Radiology, Taipei Veterans General Hospital, Taipei, Taiwan
Kang-Lung Lee
Department of Radiology, Taipei Veterans General Hospital, Taipei, Taiwan
Chia-Hung Wu
Department of Radiology, Taipei Veterans General Hospital, Taipei, Taiwan
Shu-Ting Chen
Department of Radiology, Taipei Veterans General Hospital, Taipei, Taiwan
Hsin-Hung Chen
Division of Pediatric Neurosurgery, Department of Neurosurgery, Neurological Institute, Taipei Veterans General Hospital, Taipei, Taiwan
Yi-Yen Lee
Division of Pediatric Neurosurgery, Department of Neurosurgery, Neurological Institute, Taipei Veterans General Hospital, Taipei, Taiwan
Yi-Wei Chen
Department of Oncology, Taipei Veterans General Hospital, Taipei, Taiwan
Chih-Chun Wu
Department of Radiology, Taipei Veterans General Hospital, Taipei, Taiwan
Ting-Rong Hsu
Department of Pediatrics, Taipei Veterans General Hospital, Taipei, Taiwan
Feng-Chi Chang (fcchang374@gmail.com)
Department of Radiology, Taipei Veterans General Hospital, Taipei, Taiwan

---

Research Article

Keywords: malignant primary brain tumor (MPBT), MRI, CT, IESL

Posted Date: November 9th, 2021

DOI: https://doi.org/10.21203/rs.3.rs-1016596/v1

Version of Record: A version of this preprint was published at Scientific Reports on February 2nd, 2022.
See the published version at https://doi.org/10.1038/s41598-022-05831-6.

Abstract

Background

Spinal metastasis from malignant primary brain tumor (MPBT) in pediatric is rare, often appearing as enhancing lesions on MRI. However, some indolent enhancing spinal lesions (IESL) resulting from previous treatment mimic metastasis on MRI, leading to unnecessary investigation and treatment.

Methods

In 2005-2020, we retrospectively enrolled 12 pediatric/young patients with clinical impression of spinal metastasis, and pathological diagnosis of their spinal lesions. Three patients had MPBT with IESL, and 9 patients had malignant tumors with metastases. The histopathologic diagnosis of IESL was unremarkable marrow change. We evaluated their MRI, CT, and bone scan findings.

Results

Image findings of IESL vs spinal metastasis were 1) shape: round/ovoid (3/3, 100%) vs irregular (9/9, 100%) (P= .005); 2) target-shaped enhancement: (3/3, 100%) vs (0/9, 0%) (P= .005); 3) pathologic fracture of vertebral body: (1/3, 33.3%) vs (9/9, 100%) (P= .045); 4) expansile vertebral shape (0/3, 0%) vs (9/9, 100%) (P= .005); 5) obliteration of basivertebral vein: (0/3, 0%) vs (9/9, 100%) (P= .005); 6) osteoblastic change on CT: (3/3, 100%) vs (2/9, 22.2%) (P= .034).

Conclusions

IESL in pediatrics with MPBT can be differentiated from metastasis by their image characteristics. We suggest close follow-up rather than aggressive investigation and treatment for IESL.

Background

Malignant primary brain tumors (MPBT) may metastasize through several pathways: local invasion, cerebrospinal fluid (CSF), and hematogenous or lymphangitic routes. Early neuroaxial metastasis through CSF is common, occurring in up to 53.5% glioblastoma patients and in about 33% at the initial diagnosis of medulloblastomas.[1, 2] To reach complete tumor control, craniospinal radiotherapy of the whole spinal region plus chemotherapy are the standard treatment for pediatric MPBT with leptomeningeal seeding.[3] In contrast with neuroaxial metastasis, distant extraneural metastases are rare, ranging from 0–7% depending on the brain tumor type.[4–7] Most extraneural metastases occur after craniotomy or diversionary CSF shunting, due to damage the blood-brain barrier.[8] Common distant metastatic sites of pediatric brain tumors are bone (56.3%, especially at pelvis, femur and vertebrae), visceral organs (55.5%, mostly liver and lung), and lymph nodes (25.3%).[4] Adjuvant treatment such as chemoradiotherapy or radiotherapy is favored for distant extracranial metastases.

MRI is the best imaging technique of diagnosing MPBT-associated spinal metastasis (SM) and leptomeningeal seeding.[9] An enhancing lesion of the spine on contrast-enhanced T1WI with/without adjacent soft tissue lesion is usually the crucial finding of SM. However, some indolent enhancing spinal lesions (IESL) on MRI may mimic SM.[10, 11] Histological expression of the IESL is usually unremarkable, with no malignant cells. The IESL may be the sequelae of previous radiotherapy, chemotherapy, stem cell transplantation, and medications such as corticosteroids, aromatase inhibitors, and bisphosphonates.[10, 11] Lacking an accurate diagnosis, pediatric patients with IESL may receive unnecessary invasive investigation and adjuvant treatment.

This retrospective study assessed the image findings of pathologically proven IESL of MPBT and SM of malignant tumors in pediatric and young patients, aiming to identify the differentiating features of IESL from SM and thus to improve therapeutic outcomes.

Methods

This retrospective study was approved by the institutional review board of Taipei Veterans General Hospital. All methods were carried out in accordance with relevant guidelines and regulations. Informed consents were obtained from each patient or their families to perform the MR examinations and the interventional procedures.

Patients

From 2005 to 2020, 12 pediatric or young patients with enhancing spinal lesions on MRI were enrolled (Table 1). All patients had the presumptive diagnosis of SM based on enhancing spinal lesions on MRI. The final histopathological diagnoses were 3 pediatric patients MPBT with IESL, and 9 pediatric/young patients with malignant tumors with SM. We recruited the 9 young patients with SM under 30 years of age because there were no pediatric patients with brain tumor and SM identified on spinal MRI in our institute during 2005 to 2020. We thoroughly reviewed the patients' clinical data, cancer treatment (radiotherapy, chemotherapy, and peripheral blood stem cell transplantation), surgical records, biopsy methods, and pathology results.

Table 1
Demographic characteristics of the 12 patients with enhancing spinal lesion on MRI

Characteristic	IESL (N=3)	SM (N=9)	P value
Female sex – no. (%)	1 (33.3)	7 (77.8)	0.24
Age at the initial diagnosis of primary tumor – year[†]	11.0±0.0 (11-11)	18.0±9.8 (2-29)	0.28
Age at the presence of spinal lesions – year[†]	17.0±9.5 (11-28)	19.0±9.6 (3-29)	0.60
Interval between the initial diagnosis of primary tumor and presence of spinal lesions – month[†]	75.3±113.3 (5-206)	8.1±11.8 (2-31)	0.19
Primary tumor type			**0.009**
Brain tumor – no. (%)	3 (100)	0 (0)	
Musculoskeletal malignancy – no. (%)	0 (0)	5 (55.6)	
Lung cancer – no. (%)	0 (0)	1 (11.1)	
Breast cancer – no. (%)	0 (0)	2 (22.2)	
Neuroendocrine tumors of unknown origin – no. (%)	0 (0)	1 (11.1)	
Systemic treatment of primary malignant tumors			
Chemotherapy – no. (%)	3 (100)	8 (88.9)	1.00
Peripheral blood stem cell transplantation (PBSCT) – no. (%)	1 (33.2)	2 (22.2)	1.00
Whole spine irradiation – no. (%)	3 (100)	0 (0)	**0.005**
Pathology examination method			0.18
Computed tomography (CT)-guided biopsy – no (%)	3 (100)[‡]	3 (33.3)	
Surgery – no (%)	0 (0)	6 (66.7)	

*Abbreviations: IESL = indolent enhancing spinal lesions; SM = spinal metastasis.

[†]Data are expressed as mean ± standard deviation (range).

[‡]One patient had undergone CT-guided biopsy twice, disclosing IESLs identically.

[§]One patient in the SM group had no follow-up image for the bone lesions, thus was excluded in the calculation.

[¶]One patient in the SM group was loss of follow-up after 50-months of treatment in our hospital; therefore, she was excluded in the calculation of survival rate.

Characteristic	IESL (N=3)	SM (N=9)	P value
Follow-up period after the initial diagnosis of primary tumor – month[†]	86.7±116.4 (5-220)	32.8±26.0 (2-83)	0.86
Progression or recurrence of the primary tumor – no (%)	3 (100)	5 (55.6)	0.49
Progression of the spinal lesions on magnetic resonance image (MRI)– no (%)	3 (100)	6 (75)[§]	1.00
Survival – no (%)	1 (33.3)	0 (0)[¶]	0.27
*Abbreviations: IESL = indolent enhancing spinal lesions; SM = spinal metastasis.			
[†]Data are expressed as mean ± standard deviation (range).			
[‡]One patient had undergone CT-guided biopsy twice, disclosing IESLs identically.			
[§]One patient in the SM group had no follow-up image for the bone lesions, thus was excluded in the calculation.			
[¶]One patient in the SM group was loss of follow-up after 50-months of treatment in our hospital; therefore, she was excluded in the calculation of survival rate.			

Imaging studies

Several image studies were performed in all patients because of the clinical impression of SM on MRI and CT (Table 2). Tc99m bone scan also was performed in 11 of the 12 patients. All the spinal lesions were not seen initially but in the sequential follow-up images. The spinal MRI sequences included axial and sagittal T1/T2-weighted image (T1WI/T2WI) and contrast-enhanced fat-suppressed T1WI. In the contrast enhanced T1WI, we analyzed the enhancing spinal lesions by their location (cervical, thoracic, lumbar, sacral, or whole spine), number, shape (round, ovoid, or irregular), and margin (well-defined or ill-defined). Some typical findings of SM were also evaluated, including expansile change with convex border, pathological fracture of the involved vertebral body, posterior element involvement, paraspinal soft tissue, epidural soft tissue lesion with a “draped curtain sign,” obliteration of the basivertebral vein, and presence of leptomeningeal seeding.[9, 12] We also recorded the enhancing spinal lesions that abutted a vertebral endplate or involved the corner of a vertebral body. We further analyzed the signal intensity of the lesions on T1WI, T2WI and contrast enhanced T1WI, comparing with paraspinal muscle on MRI. A special “target enhancement” pattern of the lesions on contrast enhanced T1WI was evaluated.

In the CT scan, we analyzed the lesions with either osteoblastic or osteolytic change and presence of pathologic fracture. Bone lesions with abnormal uptake on Technetium-99m methylene diphosphonate (Tc99m-MDP) bone scan also were documented.

Pathologic diagnoses

Under the clinical impression of SM, pathological assessment of the suspected metastatic bone lesions was performed to confirm the diagnosis. Tissue was obtained either by CT-guided biopsy or surgical biopsy. For CT-guided biopsy, a single long-core bony specimen was obtained with an 11-gauge Jamshidi™ bone marrow biopsy needle after localization (Fig. 1-3). Surgical biopsy was performed by wide resection of the lesion via open technique for decompressing the extradural compression. Immunohistochemical stains were used in histological studies to detect metastasis.

Statistical assessment

All statistical analyses were performed with IBM® SPSS® statistics subscription. Continuous variables were summarized as mean values with standard deviations; P values were calculated with the Mann-Whitney U test. Categorical variables were summarized as counts and percentages. P values were calculated with Fisher's exact test in two categorical variables, and via likelihood ratio for the variables with more than 3 categories. Patients with missing data in a variable were excluded from the analysis of the specified variable. All reported P values are two-sided. P values less than 0.05 were considered statistically significant.

Results

Demographic Features

Characteristics of the 3 IESL patients and the 9 SM patients are listed in Table 1. Tissue examination of 2 of the IESL cases revealed hypocellular marrow, fibrosis, and adipose tissue replacement; the other IESL case had normal marrow with nearly normal hematopoiesis. One patient with IESL had undergone repeated CT-guided biopsy in different bone lesions, disclosing similar pathology with no malignant cells. The two groups did not differ in age, gender, primary tumor origin, systemic treatment (chemotherapy, radiotherapy, peripheral blood stem cell transplantation), and biopsy methods used. The time interval from the diagnosis of primary malignant tumors to the presence of spinal lesions was 75.3±113.3 (5-206) months in the IESL group and 8.1±11.8 (2-31) months in the SM group (P= .19). No fluctuation was seen in the complete blood count of all 12 patients at the time spinal lesions were discovered. All patients in both groups had received systemic chemotherapy for the primary malignant tumor. The 3 pediatric IESL patients had undergone craniospinal radiotherapy as the management of MPBT with leptomeningeal seeding. During the follow up period, all the 3 IESL patients and 6 of the 8 SM patients (75%) had progressive change of the spinal lesions on MRI (*P*=1.0) (Figure 1-3). In addition to IESL, new scattered enhancing lesions were present over the skull of all 3 patients with MPBT in their follow-up brain MRI (Figure 2H).

Imaging findings

Image features of the bone lesions for the IESL and SM are listed in Table 2. The IESL were round or ovoid (3/3, 100%), whereas all SM lesions appeared irregular (9/9, 100%) (P= .005). Ill-defined lesion

margins were noted in 1 of the 3 IESL (33.3%), whereas all true metastases had ill-defined margins (100%) (P= .045) (Figure 3, 4).

For the associated findings of the vertebral lesions, SM had a significantly higher incidence of pathological fracture than did IESL (9/9 [100%] vs 1/3 [33.3%], P= .045); paraspinal soft tissue lesions (7/9 [77.8%] vs 0/3 [0%], P= .045); epidural soft tissue (8/9 [88.9%] vs 0/3 [0%], P= .018); expansile vertebral shape (9/9 [100%] vs 0/3 [0%], P= .005); and obliteration of the basivertebral vein (9/9 [100%] vs 0/3 [0%], P= .005) (Figure 4). The MPBT patients with IESL had more leptomeningeal seeding than did the patients with SM during their disease courses (3/3 [100%] vs 2/9 [22.2%], P= .045) (Figure 1, 2).

For MR signals, IESL had significantly more hypointense signals on T2WI than did SM (2/3, [66.7%] vs 0/0, [0%], P= .021). No difference of signal intensity was seen on T1WI and contrast enhanced T1WI between the two groups. A target enhancement pattern of the large lesions on contrast enhanced T1WI was present in all 3 IESL patients of (3/3, 100%) (Figure 1-3), but none was seen in the SM group (0/9, 0%) (P= .005).

In the CT scans, all IESL had osteoblastic change (3/3, 100%) (Fig. 1-3), whereas only 2 SM had osteoblastic change (2/9, 22.2 %) (P= .034). For the 11 of our 12 patients who accepted bone scans, there was a trend of higher incidence of uptake in SM patients (8/8, 100%) (Figure 4) than IESL patients (1/3, 33.3%) (P= .055).

Discussion

Enhancing lesions on spinal MRI is a common finding of patients with malignant tumors and spinal metastasis. Treatment-related vertebral enhancing lesions have seldom been reported, especially in pediatric patients.[10, 11, 13] Our study compared the image findings between treatment-induced IESL and true metastasis to the spine (Figure 5). The main image characteristics of IESL were 1) round/ovoid and well-defined shape; 2) osteoblastic appearance on CT; 3) target-shaped enhancement on contrast enhanced MRI T1WI; 4) hypointensity on MRI T2WI; 5) preserved basivertebral vein; 6) lack of vertebral pathological fracture, paraspinal soft tissue, and expansile vertebral change. An accurate diagnosis of these MR enhancing lesions helps to prevent unnecessary invasive investigation and to promote appropriate management.

SM from extracranial malignant tumors in pediatric patients usually presents as inhomogeneous bone lesions in the CT scan, which can be either lytic, sclerotic, or mixed. [14,15] Typical MRI characteristics of SM include expansile change of the involved vertebrae, pathological fracture, pedicle or posterior element involvement, and paraspinal/epidural mass. [9, 14, 16, 17] These lesions are often hypointense on TIWI, hyperintense on T2WI, and have partial or marked post-contrast enhancement.[14, 15, 18] A hypointense lesion with hyperintense rim on T2WI, i.e., “the halo sign,” is also an indicator of metastasis.[9] Metastatic lesions generally have avid uptake on bone scan.[15] In contrast, pediatric MPBT with distant extraneural

SM is rare. MPBT with SM have had image features like those of SM from extracranial malignant tumors.[15, 16, 19–23]

In our 3 IESL cases, neither malignant cells nor active inflammatory process was found on pathology examination. Besides, these lesions developed in the serial follow-up images but were not seen in the initial diagnosis of MPBT. These results suggest that IESL is likely a delayed response to the clinical treatment of MPBT with leptomeningeal seeding.[10, 11, 13] In the acute phase after radiotherapy and chemotherapy (within 1-2 weeks), cellular depletion and marrow edema occurs, with increased signal intensity on T2WI. Subsequently, fatty replacement and fibrosis take place, with disappearance of the red marrow. MRI then has heterogenous hyperintensity on T1WI, consistent with predominantly fat marrow. After 3-6 weeks of treatment, red marrow sometimes regenerates. The red marrow foci are hypointense on T1WI and T2WI, with variable post-contrast enhancement.[11, 13, 24, 25] Radiation-induced hematopoiesis is often patchy or band-like within the radiation portal; by contrast, hematopoiesis induced by chemotherapy, granulocyte-colony stimulating factor treatment, or hematopoietic stem cell transplantation often is diffuse, presenting as multifocal regenerating foci.[11, 13, 24, 26] In the Tc99m bone scan, hematopoietic marrow usually has no abnormal uptake, but increased uptake has been reported owing to high osteoblastic activity by the proliferation of hematopoietic cells. [25, 27] Our IESL patients had predominantly hypointense signals on T1WI and T2WI with post-contrast enhancement on MRI, and 2 of 3 had no uptake in the bone scan; these findings are like those of red marrow regeneration. However, active hyperplastic hematopoiesis was not evident in any of the pathology specimens. Therefore, we suggest that hematopoiesis is a contributing factor but cannot completely explain the mechanism of IESL.

The other possible explanation for IESL of pediatric MPBT is bone marrow ischemia/necrosis. Marrow fibrosis is induced by radiotherapy and chemotherapy, which may lead to marrow ischemia and necrosis.[28–30] Radiation-induced marrow necrosis usually is localized within the radiation portal, i.e., osteoradionecrosis, which could have occurred in our patients, as they were treated with whole spine irradiation for leptomeningeal seeding.[11] Typical image characteristics of spinal necrosis are discrete, well-defined, nonexpansile lesions, which lack soft tissue mass.[31] Osteonecrosis/infarction usually has a sclerotic appearance on CT scan, indicating calcification of the necrotic tissue or osteoblastic reparation of the focal ischemic insult.[18, 30] In MRI, these lesions often appear hypointense on T1WI and hyperintense on T2WI, which may become hypointense in late disease.[18, 31, 32] The “double line sign” is an image feature of early avascular necrosis, consists of a high-signal inner line representing hyperemic granulation and a low-signal outer parallel rim representing sclerotic bone on T2WI. [13,32] The layer of granulation tissue between necrotic and viable bone appears as rim enhancement in contrast-enhanced images.[32] One of our IESL patients had hyperintense spinal lesions with “double line sign” on T2WI and ring enhancement on post-contrast T1WI (Figure 1E, G), which is compatible with the common finding of bone infarction/necrosis.[13, 32] The Tc99m bone scan demonstrates variable uptake in bone infarcts and no uptake in the necrotic regions.[18, 33] In 2 of our 3 IESL patients, no uptake was evident on the bone

scan, which is compatible with ischemia/necrosis or hematopoiesis.[18, 25, 33] However, some hot spots were seen in 1 IESL patient's scan; this finding may be related to the uncommon presentation of bone infarct or focal hematopoiesis.[27, 33] In contrast, all SM patients had significantly increased uptake in the bone scan.

In our study, the imaging presentation of all IESL was mostly compatible with bone infarction/necrosis. Irradiation-induced cellular depletion and marrow fibrosis had been reported to progressively worsen over time, especially after 6 months of radiotherapy, which might explain the progressive change in our IESL. [28] Therefore, we favor dynamic marrow response with fibrosis and delayed ischemic/necrotic bone insult as the major mechanism of IESL in pediatric MPBT patients who were treated with craniospinal irradiation and chemotherapy. This view is compatible with the histologic findings of hypocellular marrow with fat replacement and fibrosis in 2 of our 3 IESL patients. The pathology finding in the other IESL patient was nearly normal hematopoiesis, which can be explained by the combination of early infarction followed by late marrow conversion.

By close examination, a target enhancement pattern of larger lesions on contrast enhanced T1WI was seen consistently in the IESL. The peripheral rim enhancement has been reported by Tang *et al*.[32] in osteonecrosis, while the target enhancing pattern has not been described. We suggest that the reparative process of the outer vascular bone marrow to the inner ischemic insult contributes to this layered enhancement. We also hypothesize that the peripheral enhancement is related to red marrow regeneration, and the central enhancing foci are composed of a fatty focus. [25, 34]

Our study has limitations. First, it is a retrospective study with a modest number of cases. Second, all IESL were found in pediatric patients with MPBT; we could not find MPBT with SM on MRI in our institute for comparison. As mentioned previously, SM from MPBT is extremely rare, and their image characteristics are much the same as those from extracranial malignant tumors. [15, 16, 19–23] Their similar image feature supports our nine SM patients being representative of all "true-metastasis" when comparing to IESL from MPBT. Further study comparing IESL and SM from MPBT may be considered. Third, although not reaching significance statistically, the IESL group had longer time intervals between the diagnosis of primary tumor and presence of spinal lesions. This is possibly related to the small number of cases, knowing that one IESL patient had his spinal lesions developed 17 years after the initial diagnosis of brain tumor, which is much longer than the other two IESL patients. Fourth, all IESL patients had received whole-spine irradiation, while none of the SM patients had prior spinal radiotherapy. It is noteworthy that whole-spine irradiation is commonly performed in MPBT due to the high incidence of neuroaxial metastasis; by contrary, spinal irradiation is not routinely performed in extracranial malignancy until the occurrence of spinal metastasis. Fifth, we did not analyze the difference between IESL and SM with advanced MRI techniques, such as dynamic contrast-enhanced T1WI, chemical-shift (in-out phase), diffusion-weighted imaging, and perfusion study.[35, 36] At last, we did not perform biopsies for all lesions with abnormal MRI signal, which may reflect hesitancy of practitioners to avoid repeated invasive procedure in pediatric patients.

In conclusion, indolent enhancing spinal lesions of malignant primary brain tumor in pediatric patients is related to treatment-induced delayed bone marrow change. We suggest that ischemic insult, such as bone infarction or necrosis, is the main mechanism responsible. IESL in pediatric patients with malignant primary brain tumors can be differentiated from spinal metastasis by their image characteristics. We recommend close follow-up rather than aggressive investigation and treatment for these IESL.

Declarations

Author contributions

FCC conceptualized this study, critically revised the manuscript, supervising data acquisition and data analysis. HWW was a major contributor in writing the manuscript, data acquisition, data analysis, visualization of the data, and prepared figures 1-5. SCL performed histological examination of the bony specimens. CLW performed CT-guided biopsy of the bone lesions. KLL supervised statical analysis and interpretation of the data. CHW, STC, HHC, YYL, YWC, CCW, TRH contributed to the study design, and supervised article drafting. All authors read, revised, and approved the final manuscript.

Competing interests

The authors declare that they have no competing interests.

Data availability

The datasets generated during and/or analysed during the current study are available from the corresponding author on reasonable request.

Approval for human experiments

This retrospective study was approved by the institutional review board of Taipei Veterans General Hospital (IRB-TPEVGH No.: 2021-07-005BC). Written informed consent was obtained from all subjects (patients or their families) in this study.

Acknowledgements

This research was co-sponsored by Taipei Veterans General Hospital (grant number: V110C-037 [to FCC]), Veterans General Hospitals and University System of Taiwan Joint Research Program (grant number: VGHUST 110-G1-5-2 [to FCC]), Ministry of Science and Technology of Taiwan (grant number: MOST 110-2314-B-075-032 [to FCC]; MOST 110-2314-B-075-005 [to CHW]) and Vivian W. Yen Neurological Foundation [to FCC and CHW]. All authors declare no competing financial interests.

References

1. Wright, C. H. *et al*. Diagnosis, treatment, and survival in spinal dissemination of primary intracranial glioblastoma: systematic literature review. *J Neurosurg Spine*. **31(5),** 723-732 (2019).
2. Millard, N. E., De Braganca K. C. Medulloblastoma. *J Child Neurol.* **31(12),** 1341-1353 (2016).
3. Packer, R. J. *et al*. Treatment of children with medulloblastomas with reduced-dose craniospinal radiation therapy and adjuvant chemotherapy: A Children's Cancer Group Study. *J Clin Oncol.* **17(7),** 2127 (1999).
4. Rickert, C.H. Extraneural metastases of paediatric brain tumours. *Acta Neuropathol*. **105(4),** 309-327 (2003).
5. Houston, S. C., Crocker, I. R., Brat, D. J., Olson, J. J. Extraneural metastatic glioblastoma after interstitial brachytherapy. *Intl J Rad Onc Biophys.* **48(3),** 831-836 (2000).
6. Newton, H. B., Henson, J., Walker, R.W. Extraneural metastases in ependymoma. *J Neuro-oncol*. **14(2),** 135-142 (1992).
7. Dalle Ore, C. L. *et al*. Meningioma metastases: incidence and proposed screening paradigm. *J Neurosurg*. **132(5),** 1447-1455 (2019).
8. Hoffman, H. J., Duffner, P. K. Extraneural metastases of central nervous system tumors. *Cancer*. **56(S7),** 1778-1782 (1985).
9. Shah, L. M., Salzman, K.L. Imaging of spinal metastatic disease. *Intl J Surg Oncol*. 2011 (2011).
10. Hwang, S., Panicek, D. M. Magnetic resonance imaging of bone marrow in oncology, Part 2. *Skeletal Radiol*. **36(11),** 1017-1027 (2007).
11. Ollivier, L., Gerber, S., Vanel, D., Brisse, H., Leclere, J. Improving the interpretation of bone marrow imaging in cancer patients. *Cancer Imaging*. **6(1),** 194-198 (2006).
12. Aydinli, U. *et al*. Evaluation of lung cancer metastases to the spine. *Acta Orthop Belg*. **72(5),** 592-597 (2006).
13. Daldrup-Link, H. E., Henning, T., Link, T. M. MR imaging of therapy-induced changes of bone marrow. **17(3),** 743-761 (2007).
14. Isaac, A., Dalili, D., Dalili, D., Weber, M. A. State-of-the-art imaging for diagnosis of metastatic bone disease. *Radiologe*. **60(Suppl 1),** 1-16 (2020).
15. Goodwin, C. R. *et al*. Extraneural glioblastoma multiforme vertebral metastasis. *World Neurosurg*. **89,** 578-582.e3 (2016).
16. Petrirena, G. J. *et al*. Recurrent extraneural sonic hedgehog medulloblastoma exhibiting sustained response to vismodegib and temozolomide monotherapies and inter-metastatic molecular heterogeneity at progression. *Oncotarget*. **9(11),** 10175-10183 (2018).
17. Zaghouani, H. *et al*. Vertebral metastases from intracranial meningioma. *Acta Radiol Short Rep*. **3(4),** 2047981613494199 (2014).
18. Murakami, H., Kawahara, N., Gabata, T., Nambu, K., Tomita, K. Vertebral body osteonecrosis without vertebral collapse. *Spine*. **28(16),** E323-328 (2003).

19. Rajagopalan, V., El Kamar, F. G., Thayaparan, R., Grossbard, M.L. Bone marrow metastases from glioblastoma multiforme – A case report and review of the literature. *J Neurooncol*. **72(2),** 157-161 (2005).
20. Marsecano, C. *et al*. Systemic metastases from central nervous system ependymoma: case report and review of the literature. *Neuroradiol J*. **30(3),** 274-280 (2017).
21. Moelleken, S. M., Seeger, L. L., Eckardt, J. J., Batzdorf, U. Myxopapillary ependymoma with extensive sacral destruction: CT and MR findings. *J Comput Assist Tomogr.* **16(1),** 164-166 (1992).
22. Al-Ali, F. *et al*. Oligodendroglioma metastatic to bone marrow. *AJNR Am J Neuroradiol*. **26(9),** 2410-2414 (2005).
23. Lummus, S. C. *et al*. Massive dissemination from spinal cord gangliogliomas negative for BRAF V600E: report of two rare adult cases. *Am J Clin Pathol*. **142(2),** 254-260 (2014).
24. Chan, B. Y., Gill, K. G., Rebsamen, S. L., Nguyen, J. C. MR imaging of pediatric bone marrow. *Radiographics*. **36(6),** 1911-1930 (2016).
25. Shigematsu, Y. *et al*. Distinguishing imaging features between spinal hyperplastic hematopoietic bone marrow and bone metastasis. *AJNR Am J Neuroradiol*. **35(10),** 2013-2020 (2014).
26. Altehoefer, C. *et al*. Prospective evaluation of bone marrow signal changes on magnetic resonance tomography during high-dose chemotherapy and peripheral blood stem cell transplantation in patients with breast cancer. *Invest Radiol*. **32(10),** 613-620 (1997).
27. Sato, T., Kunimatsu, J., Watanabe, R., Kato, O. A Rare Cause of Multiple Bone Lesions: Metastasis or Not?. *Am J Med.* **129(3),** e15-16 (2016).
28. Curi, M. M., Cardoso, C. L., De Lima, H. G., Kowalski, L. P., Martins, M. D. Histopathologic and histomorphometric analysis of irradiation injury in bone and the surrounding soft tissues of the jaws. *J Oral Maxillofac Surg*. **74(1),** 190-199 (2016).
29. Fu, B. *et al*. The clinical importance of moderate/severe bone marrow fibrosis in patients with therapy-related myelodysplastic syndromes. *Ann Hematol*. **92(10),** 1335-1343 (2013).
30. Alhilali, L., Reynolds, A. R., Fakhran, S. Osteoradionecrosis after radiation therapy for head and neck cancer: differentiation from recurrent disease with CT and PET/CT imaging. *AJNR Am J Neuroradiol*. **35(7),** 1405-1411 (2014).
31. Maheshwari, P. R., Nagar, A. M., Prasad, S. S., Shah, J. R., Patkar, D. P. Avascular necrosis of spine: a rare appearance. **29(6),** E119-122 (2004).
32. Tang, Y. M., Jeavons, S., Stuckey, S., Middleton, H., Gill, D. MRI features of bone marrow necrosis. *AJR Am J Roentgenol*. **188(2),** 509-514 (2007).
33. Rao, S., Solomon, N., Miller, S., Dunn, E. Scintigraphic differentiation of bone infarction from osteomyelitis in children with sickle cell disease. *J Pediatr*. **107(5),** 685-688 (1985).
34. Shah, L. M., Hanrahan, C. J. MRI of spinal bone marrow: part 1, techniques and normal age-related appearances. *AJR Am J Roentgenol*. **197(6),** 1298-1308 (2011).

35. Chu, S. *et al*. Measurement of blood perfusion in spinal metastases with dynamic contrast-enhanced magnetic resonance imaging: evaluation of tumor response to radiation therapy. *Spine.* **38(22),** E1418-E1424 (2013).
36. Suh, C. H. *et al*. Diagnostic performance of in-phase and opposed-phase chemical-shift imaging for differentiating benign and malignant vertebral marrow lesions: a meta-analysis. *AJR Am J Roentgenol*. **211(4),** W188-197 (2018).

Tables

Table 1. Demographic characteristics of the 12 patients with enhancing spinal lesion on MRI			
Characteristic	**IESL (N=3)**	**SM (N=9)**	**P value**
Female sex – no. (%)	1 (33.3)	7 (77.8)	0.24
Age at the initial diagnosis of primary tumor – year[†]	11.0±0.0 (11-11)	18.0±9.8 (2-29)	0.28
Age at the presence of spinal lesions – year[†]	17.0±9.5 (11-28)	19.0±9.6 (3-29)	0.60
Interval between the initial diagnosis of primary tumor and presence of spinal lesions – month[†]	75.3±113.3 (5-206)	8.1±11.8 (2-31)	0.19
Primary tumor type			**0.009**
Brain tumor – no. (%)	3 (100)	0 (0)	
Musculoskeletal malignancy – no. (%)	0 (0)	5 (55.6)	
Lung cancer – no. (%)	0 (0)	1 (11.1)	
Breast cancer – no. (%)	0 (0)	2 (22.2)	
Neuroendocrine tumors of unknown origin – no. (%)	0 (0)	1 (11.1)	
Systemic treatment of primary malignant tumors			
Chemotherapy – no. (%)	3 (100)	8 (88.9)	1.00
Peripheral blood stem cell transplantation (PBSCT) – no. (%)	1 (33.2)	2 (22.2)	1.00
Whole spine irradiation – no. (%)	3 (100)	0 (0)	**0.005**
Pathology examination method			0.18
Computed tomography (CT)-guided biopsy – no (%)	3 (100)[‡]	3 (33.3)	
Surgery – no (%)	0 (0)	6 (66.7)	
Follow-up period after the initial diagnosis of primary tumor – month[†]	86.7±116.4 (5-220)	32.8±26.0 (2-83)	0.86
Progression or recurrence of the primary tumor – no (%)	3 (100)	5 (55.6)	0.49
Progression of the spinal lesions on magnetic resonance image (MRI)– no (%)	3 (100)	6 (75)[§]	1.00
Survival – no (%)	1 (33.3)	0 (0)[¶]	0.27

*Abbreviations: IESL = indolent enhancing spinal lesions; SM = spinal metastasis.

†Data are expressed as mean ± standard deviation (range).

‡One patient had undergone CT-guided biopsy twice, disclosing IESLs identically.

§One patient in the SM group had no follow-up image for the bone lesions, thus was excluded in the calculation.

¶One patient in the SM group was loss of follow-up after 50-months of treatment in our hospital; therefore, she was excluded in the calculation of survival rate.

Table 2. Image features of the 12 patients with enhancing spinal lesions on MRI				
Image features	**IESL (N=3)**	**SM (N=9)**	**P value**	**Odds ratio**
Magnetic resonance image (MRI)				
Lesion location			0.51	
Confined to T/L-spine – no. (%)	0 (0)	3 (33.3)		
Whole spine – no. (%)	3 (100)	6 (66.7)		
Lesion number			0.12	
1-10 – no. (%)	0 (0)	5 (55.6)		
11-20 – no. (%)	3 (100)	4 (44.4)		
21-30 – no. (%)	2 (66.7)	2 (22.2)		
31 – no. (%)	0 (0)	1 (11.1)		
Irregular lesion shape	0 (0)	0 (100)	**0.005**	
Ill-defined lesion margin	1 (33.3)	9 (100)	**0.045**	
Abutting endplate – no. (%)	2 (66.7)	9 (100)	0.25	
Corner involvement – no. (%)	3 (100)	7 (77.8)	1.00	
Posterior element involvement – no. (%)	2 (66.7)	8 (88.9)	0.46	0.25
Target-shaped enhancement – no. (%)	3 (100)	0 (0)	**0.005**	
Pathologic fracture – no. (%)	1 (33.3)	9 (100)	**0.045**	
Epidural soft tissue – no. (%)	0 (0)	8 (88.9)	**0.018**	
Paraspinal soft tissue – no. (%)	0 (0)	7 (77.8)	**0.045**	
Expansile vertebral shape– no. (%)	0 (0)	9 (100)	**0.005**	
Obliteration of basivertebral vein – no. (%)	0 (0)	9 (100)	**0.005**	
T1WI[‡]			-	
Hyperintensity or isointensity – no. (%)	0 (0)	0 (0)		
Hypointensity – no. (%)	3 (100)	9 (100)		
T2WI			**0.021**	
Hyperintensity – no. (%)	1 (33.3)[†]	6 (66.7)		
Isointensity – no. (%)	0 (0)	3 (33.3)		
Hypointensity – no. (%)	2 (66.7)	0 (0)		

Contrast-enhanced T1WI			-
Enhancement – no. (%)	3 (100)	9 (100)	
No enhancement – no. (%)	0 (0)	0 (0)	
Leptomeningeal seeding – no. (%)	3 (100)	2 (22.2)	**0.045**
Computed tomography (CT)			**0.034**
Osteoblastic – no. (%)	3 (100)	2 (22.2)	
Osteolytic – no. (%)	0 (0)	6 (66.7)	
Mixed – no. (%)	0 (0)	1 (11.1)	
Tc99m bone scan			0.055
Abnormal uptake – no. (%)	1(33.3)	8 (100)[‡]	
No abnormal uptake – no. (%)	2 (66.7)	0 (0)	

*Abbreviations: IESL = indolent enhancing spinal lesions; SM = spinal metastasis; MRI = magnetic resonance image; T1WI = T1-weighted image; T2WI = T2-weighted image.

[†]One IESL patient had lesions with both high and low signal intensity on T2WI. Since most lesions were T2 hyperintensity, this patient was assigned to this group.

[‡]Tc99m bone scan was not performed in one SM patient.

Figures

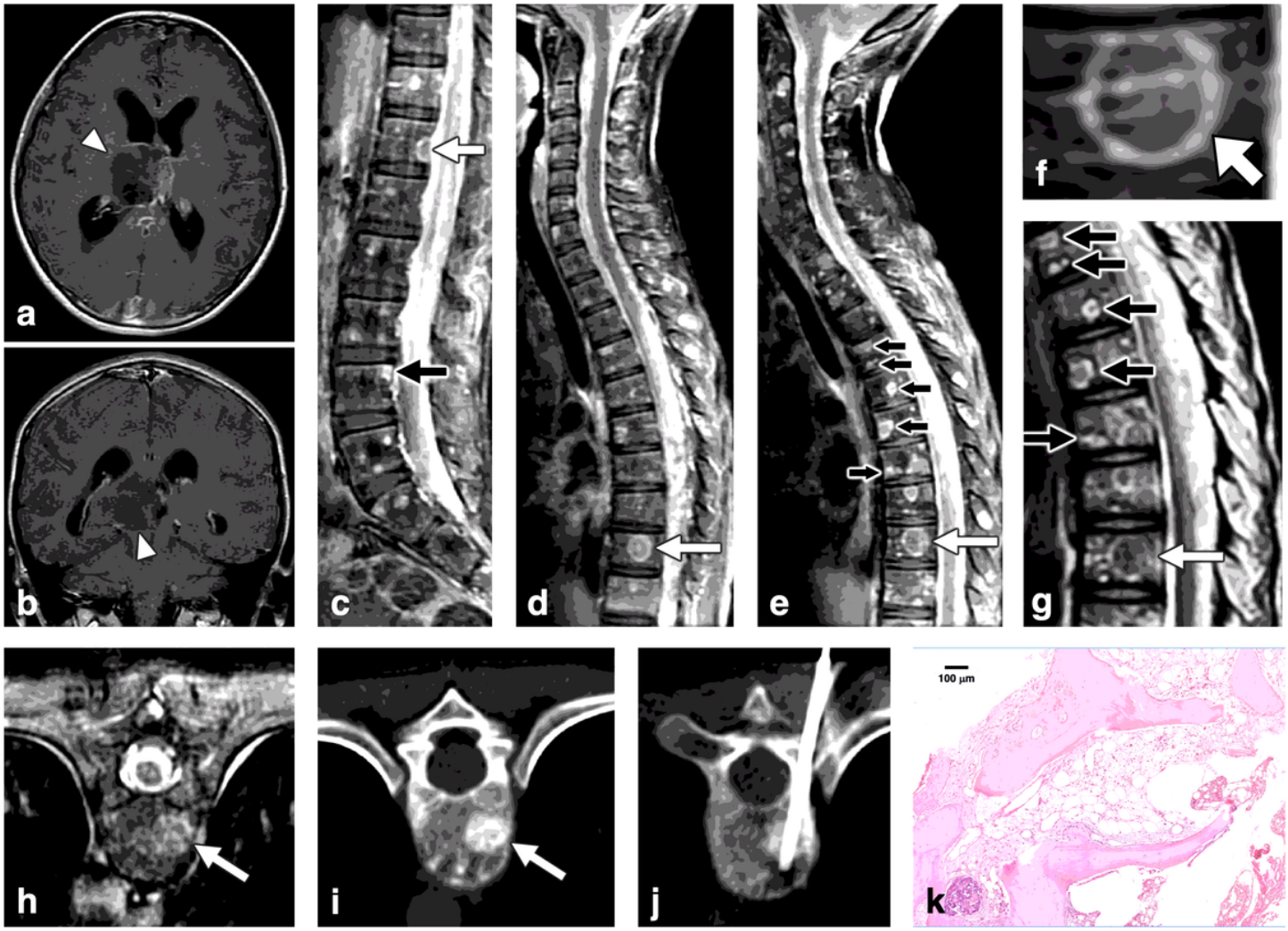

Figure 1

Indolent Enhancing Spinal Lesion (IESL) - Case 1. An 11-year-old girl with anaplastic astrocytoma (2016 WHO grade III) over the right thalamus (a, b) was treated with partial tumor removal, radiotherapy, and chemotherapy. Four months after the surgery, sagittal contrast enhanced T1WI revealed diffuse leptomeningeal seeding and multiple enhancing lesions over the whole spine (c, d). Target enhancement (d, arrow), ring enhancement (c, white arrow) and corner involvement (c, black arrow) were present. In the follow-up MRI 6 months after brain tumor surgery, sagittal contrast enhanced T1WI of the cervical to middle thoracic spine revealed progression of the lesions (e). A target-enhancing pattern was specified at T10 level (d, e, white arrow; magnified in f), which appeared hypointense on T2WI (g, white arrow). Coexisting lesions with ring enhancement on T1WI (e, black arrow), and hyperintensity with “double line sign” on T2WI were also noted (g, black arrow). The T10 target-enhancing lesion on axial contrast enhanced T1WI (h) revealed osteoblastic change on CT scan (i). The first CT-guided biopsy disclosed no histologic evidence of malignancy (j). A week later, the second CT-guided biopsy revealed hypocellular marrow tissue and bone dust (H&E staining) (k).

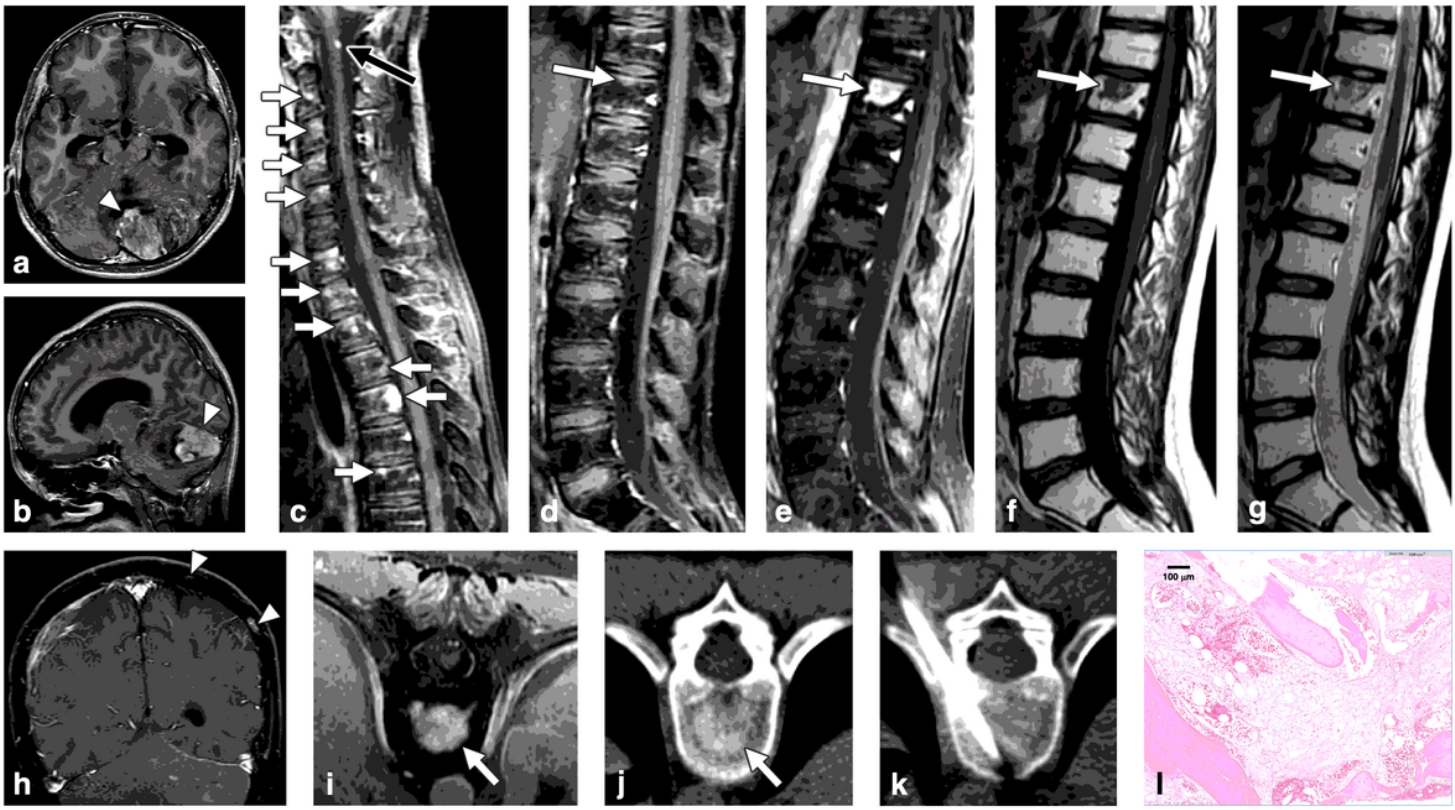

Figure 2

Indolent Enhancing Spinal Lesion (IESL) - Case 2. An 11-year-old boy with medulloblastoma of the cerebellum (a, b) had undergone surgical resection and chemoradiotherapy. Sagittal contrast enhanced T1WI revealed multiple enhancing foci in the cervical to the thoracic spine 15 months after the diagnosis (c, d). Focal leptomeningeal seeding was noted in the C1 level (c, black arrow). In the follow-up MRI 33 months after brain tumor surgery, sagittal contrast enhanced T1WI revealed significantly progressive change of the lesion at vertebrae T11 with target enhancement pattern (e, arrow). The lesion had hypointensity on T1WI (f) and hypointensity on T2WI (g). Several enhancing lesions were also present in at the temperoparietal skull bone of the brain MRI (h). On axial images, the T11 lesion had strong enhancement on contrast enhanced MRI T1WI (i), and osteoblastic change on the CT scan (j). CT-guided biopsy of the T11 lesion showed mild marrow fibrosis, adipose tissue filled in the marrow spaces, and scattered hematopoietic cells (H&E staining) (k, l).

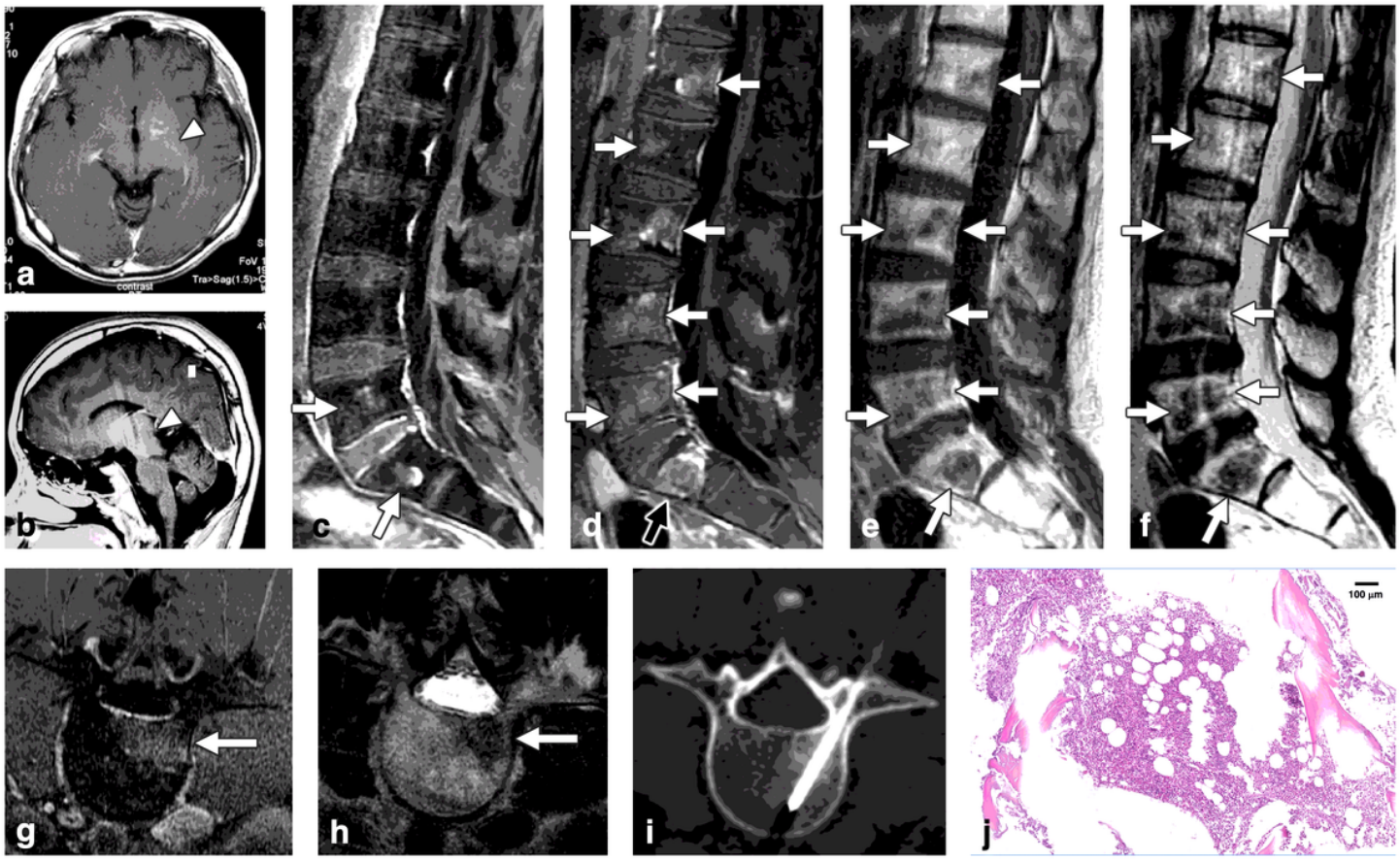

Figure 3

Indolent Enhancing Spinal Lesion (IESL) - Case 3. An 11-year-old boy had germ cell tumor over the thalamus to the hypothalamus (a, b). He had completed radiotherapy and chemotherapy. In 17 years after the initial diagnosis, follow-up spinal MRI revealed enhancing lesions in lumbosacral region on sagittal contrast-enhanced T1WI (c, arrow). Progressive change of the lesions over the whole spine was seen a year later (d, e, f). These lesions appeared well enhanced on contrast enhanced T1WI (d, g), with hypointensity on T1WI (e) and T2WI (f, h). A target enhancement pattern was also identified (d, black arrow). CT-guided biopsy of the L4 lesion revealed nearly normal hematopoiesis (H&E staining) (i, j).

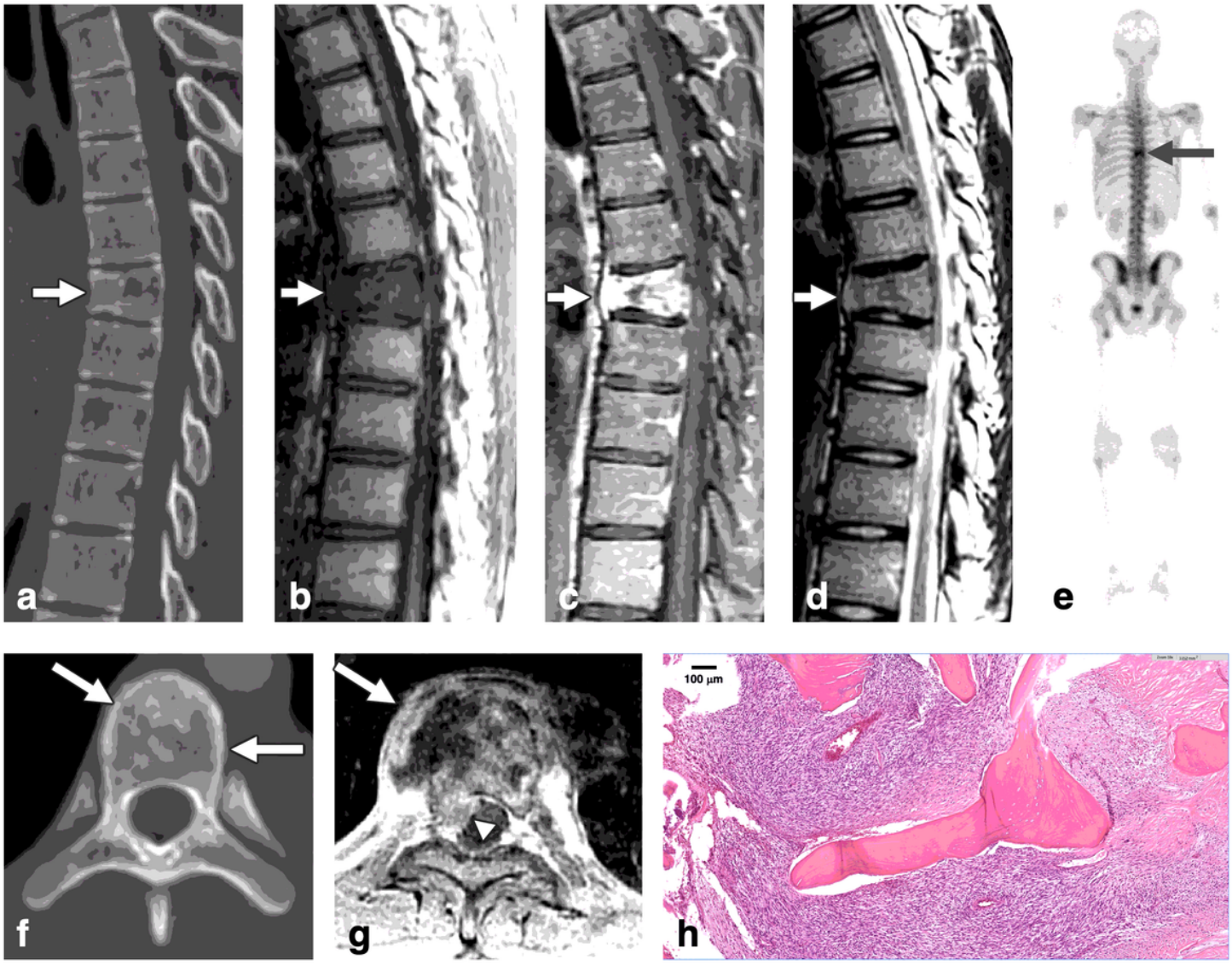

Figure 4

A Case of Spinal Metastasis (SM) A 15-year-old male with synovial sarcoma over the left knee and pulmonary metastasis, had undergone tumor resection and radiotherapy. Twenty-two months after the initial diagnosis was made the follow-up chest CT revealed an osteolytic lesion at T7 spine with partial collapse of the vertebral body (a). MRI revealed hypointensity on T1WI (b), strong enhancement on contrast enhanced T1WI (c), and isointensity on T2WI (d). Tc99m bone scan revealed avid uptake over T7 (e, arrow). The T7 lesion appeared osteolytic on axial CT image (f). The axial contrast enhanced MRI T1WI at T7 level revealed enhancing lesions with expansile change, paraspinal soft tissue (g, arrow), epidural soft tissue (g, arrowhead), and obliteration of the basivertebral vein. Bone metastasis was histologically proved by T7 corpectomy (H&E staining) (h).

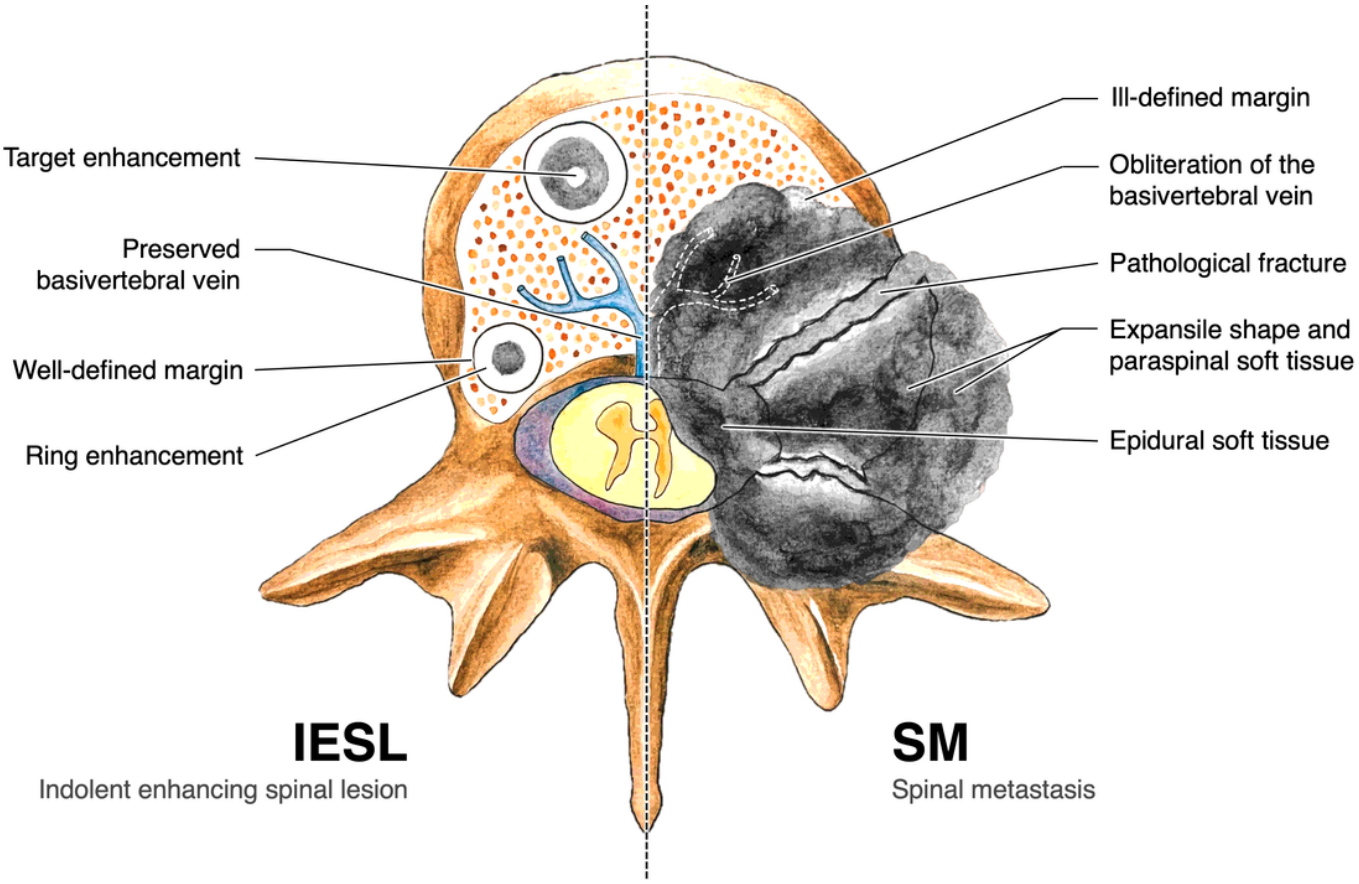

Figure 5

Indolent Enhancing Spinal Lesion versus Spinal Metastasis Comparison of the image characteristics of IESL and SM. IESLs tend to 1) be round/ovoid and well-defined; 2) have osteoblastic appearance on CT; 3) show target-shaped enhancement on contrast enhanced MRI; 4) have preserved basivertebral vein; 5) lack of vertebral pathological fracture, paraspinal soft tissue, and expansile vertebral shape.